

# Computational Study on Homolytic Bond Energies of the Ag–X (X = C, O, and H) Complexes and Hammett-Type Analysis of Reactivity

Lei Wu, Shi-Ya Tang,\* and Shaodong Zhou\*

Cite This: *ACS Omega* 2021, 6, 34904–34911

Read Online

ACCESS |



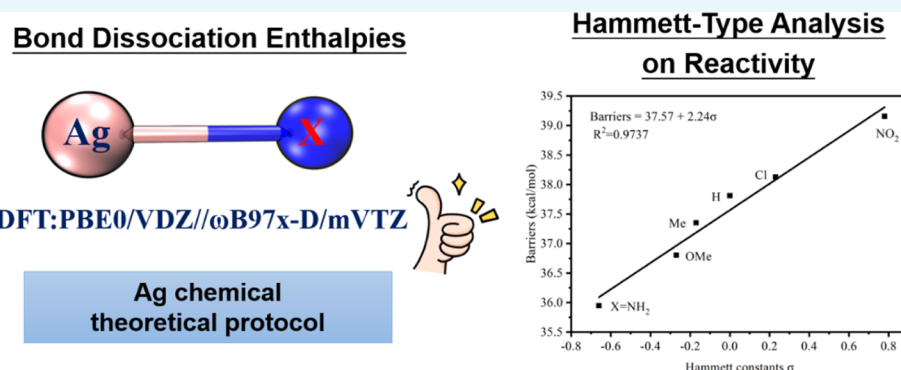
Metrics &amp; More



Article Recommendations



Supporting Information



**ABSTRACT:** Thirty-seven calculation methods were benchmarked against the available experimental bond lengths and energies data regarding the Ag–X bonds. The theoretical protocol PBE0/VDZ// $\omega$ B97x-D/mVTZ was found to be capable of accurately predicting the homolytic bond dissociation energies (BDEs) of Ag–X complexes with a precision of 1.9 kcal/mol. With the available method in hand, a wide range of different Ag–X BDEs were estimated. BDE(Ag–CH<sub>2</sub>X), BDE(Ag–PhX), BDE(Ag–OPhX), and BDE(Ag–OCOPhX) (X = NH<sub>2</sub>, OMe, Me, H, Cl, and NO<sub>2</sub>) were found to be in the ranges of 27–47, 51–54, 19–39, and 64–70 kcal/mol, respectively. Subsequently, Hammett-type analysis was carried out with reactivity parameters. Good positive linear relationships were found for BDE of Ag–O bands and decarboxylation barriers of Ag–OCOPhX with the Hammett constant  $\sigma$ . It suggested that electron-donating substituents could promote either the homolytic cleavage of the Ag–OPhX bond to undergo a radical process or Ag–OCOPhX decarboxylation. Moreover, ligand effects on Ag–H bonds were investigated using BDE(Ag–H) and related NPA charges on Ag. In the case of P-ligands, carbene ligands, and other small molecule ligands (i.e., CO, CO<sub>2</sub>, and H<sub>2</sub>O), a good negative linear relationship was found. In contrast, N-ligands could have a reverse effect. Understanding the intrinsic relationships of BDE(Ag–X) with related reactivity parameters might help gain insights into the structure–reactivity relationships in Ag–X-assisted C–H activation/decarboxylation.

## 1. INTRODUCTION

Silver-catalyzed/-assisted functionalization processes have emerged as a promising field in organic reactions, such as C–H activation and decarboxylation.<sup>1–4</sup> Indeed, Ag reagents play a crucial role in these processes during which the breaking and formation of the Ag–X (X = C, O, and H) bonds may take place.<sup>5–7</sup> Accordingly, a fundamental understanding of the factors controlling the Ag–X bond strength is of great importance regarding rational design of Ag catalysts. However, limited by insufficient experimental methods, there exist few studies dealing with the thermodynamic parameters as well as the reactivities of various Ag–X bonds. With the improvement of the supercomputing and quantum chemical calculation methods, theoretical methods have become an effective way to accurately evaluate these features, that is, bond energies. To this end, much effort has already been made. The Minenkov group<sup>8</sup> has systematically studied the thermodynamic properties of a series of simple silver salts in the gas phase using the

first-principles theory; the DLPNO-CCSD(T) method was used to calculate the bond energies of Ag–X (X = H, F, Cl, Br, I, CN, etc). However, for much larger Ag complexes, the calculation with the coupled cluster method could be unaffordably time-consuming. As an alternative, density functional theory (DFT) has been widely employed in both kinetic and thermodynamic calculations. For example, B3LYP/ECP28MWB was utilized by the Siu group to evaluate the binding energies between Ag(I) and neutral ligands (such as H<sub>2</sub>O, CH<sub>3</sub>OH, CH<sub>3</sub>CN, and amide) with a precision of 4–6

Received: October 6, 2021

Accepted: November 18, 2021

Published: December 7, 2021



**Table 1.** Calculated Bond Lengths of Ag–X with Various Methods and Basis Sets (See Table S2 for More Detailed Basis Set Descriptions and References) and Deviation from Experimental Values

methods	bond length (Å)							MSE	MAE	RMSE
	Ag–H	Ag–O	Ag–F	Ag–Cl	Ag–OH	Ag–Br	Ag–I			
experimental	1.617	2.003	1.983	2.281	2.016	2.393	2.545			
1 B3LYP def2-SVP	1.633	2.025	2.011	2.330	2.040	2.439	2.608			
	[0.016]	[0.022]	[0.027]	[0.050]	[0.024]	[0.046]	[0.063]	0.035	0.035	0.039
2 B3LYP 6-31 + G(d), def2-SVP	1.624	2.007	1.980	2.317	2.019	2.439	2.608			
	[0.007]	[0.004]	[−0.004]	[0.036]	[0.003]	[0.046]	[0.063]	0.022	0.023	0.033
3 B3LYP 6-311++G(2d,2p), def2-TZVP	1.619	2.017	2.008	2.323	2.034	2.434	2.593			
	[0.002]	[0.014]	[0.025]	[0.042]	[0.018]	[0.041]	[0.049]	0.027	0.027	0.032
4 B3LYP def2-TZVP	1.619	2.007	1.997	2.308	2.025	2.434	2.593			
	[0.002]	[0.004]	[0.014]	[0.027]	[0.009]	[0.041]	[0.049]	0.021	0.021	0.027
5 B3LYP VDZ	1.623	1.994	1.973	2.312	2.011	2.434	2.603			
	[0.006]	[−0.009]	[−0.010]	[0.031]	[−0.050]	[0.041]	[0.057]	0.016	0.023	0.030
6 B3LYP aVTZ	1.616	1.999	1.992	2.306	2.020	2.425	2.585			
	[−0.001]	[−0.004]	[0.009]	[0.025]	[0.004]	[0.032]	[0.040]	0.015	0.017	0.022
7 BP86 VDZ	1.610	1.959	1.968	2.292	2.004	2.412	2.580			
	[−0.007]	[−0.044]	[−0.015]	[0.011]	[−0.012]	[0.019]	[0.035]	−0.002	0.021	0.024
8 PBE0 VDZ	1.621	1.989	1.968	2.294	2.000	2.412	2.578			
	[0.004]	[−0.014]	[−0.015]	[0.013]	[−0.016]	[0.019]	[0.033]	0.003	0.016	0.018

kcal/mol.<sup>9</sup> The O'Hair group<sup>10</sup> found that M06 could accurately estimate the Ag–CH<sub>3</sub> bond energies, and a series of Ag–C<sub>alkyl</sub> bonds were investigated using this method. Furthermore, the Hii group<sup>11</sup> and the Chattaraj<sup>12</sup> group have studied the bond energies of Ag–carbene and Ag–bipyridine and neutral small molecule ligands such as H<sub>2</sub>, N<sub>2</sub>, CO, and CO<sub>2</sub> using BP86 and PBE0, respectively. However, if not controversial, the suitable DFT methods for the prediction of the Ag–X bond energies may remain unclear. Moreover, the essential correlation between the reactivity of the Ag complex and the electronic structure of the Ag–X bond is highly demanding.

In this work, a systematic theoretical study on the relationship between BDE(Ag–X) and the reactivity parameters was carried out. At first, different density functionals (see Table S1) were assessed by predicting the homolytic BDEs of Ag–X (X = C, O, and H) against the available experimental bond length and energetic data. Furthermore, with the selected method, an extensive range of different Ag–X BDEs were established. Last but not the least, the Hammett constants, decarboxylation barriers of Ag–OCOPhX, and ligand effects on Ag–H were discussed in detail. Understanding the intrinsic relationships between BDE(Ag–X) and the related reactivity parameters might help gain insights into the structure–activity relationships in Ag–X-assisted C–H activation/decarboxylation.

## 2. RESULTS AND DISCUSSION

**2.1. Benchmark Calculations on the Structures.** For silver compounds Ag–X (X = H, O, OH, F, Cl, Br, and I), experimental bond lengths as benchmark values were selected from the CRC Handbook of Chemistry and Physics<sup>13</sup> as shown in Table 1. The well-documented method B3LYP with a series of basis sets was first tested to examine its accuracy on the geometry optimization. Unfortunately, the bond lengths were overestimated by B3LYP. Moreover, a flexible basis set could be beneficial to predict the structures of Ag–X compounds (Table 1, entries 1–6). Despite this, VDZ (cc-pVDZ for H, O, F, and Cl; cc-pVDZ-PP for Br, I, and Ag,

Table S2) was employed for the further calculations with different functionals instead of the time-consuming 3ξ def2-TZVP and aVTZ (aug-cc-pVTZ for H, O, F, and Cl; aug-cc-pVTZ-PP for Br, I, and Ag, Table S2) basis sets. Next, BP86 and PBE0 previously used by Hii and Chattaraj were employed as well as other 34 DFT functionals involving different rungs of the Jacob ladder.<sup>14,15</sup> The results are presented in Tables 1 and S3. Remarkably, PBE0/VDZ performed the best with a RMSE of 0.018 Å. More detailed results are also shown in Figure S1.

**2.2. Benchmark Calculations for BDE(Ag–X).** The BDEs (eq 1) of Ag–X compounds could be estimated according to eq 2



$$\begin{aligned} \text{BDE}(\text{Ag-X}) &= E(\text{Ag}) + E(\text{X}) - E(\text{AgX}) + H_c(\text{Ag}) \\ &+ H_c(\text{X}) - H_c(\text{AgX}) \end{aligned} \quad (2)$$

where  $E(\text{Ag})$ ,  $E(\text{X})$ , and  $E(\text{AgX})$  are the single-point energies of the Ag, X, and AgX molecules, respectively, and  $H_c(\text{Ag})$ ,  $H_c(\text{X})$ , and  $H_c(\text{AgX})$  are the energies of thermal correction to enthalpy of Ag, X, and AgX molecules, respectively.

The signed error (SE) of each Ag–X bond length discussed in this paper was calculated according to eq 3

$$\text{SE} = R_{\text{computed}} - R_{\text{standard}} \quad (3)$$

where  $R_{\text{computed}}$  is the bond length calculated between the Ag atom and the directly connected bonding atom and  $R_{\text{standard}}$  is the experimental bond length, which is shown in Table 1. Similarly, the SE of each Ag–X BDE can be calculated according to eq 4

$$\text{SE} = \text{BDE}_{\text{computed}} - \text{BDE}_{\text{standard}} \quad (4)$$

where  $\text{BDE}_{\text{computed}}$  is the BDE calculated using MP2 and DFT methods according to eq 1 and  $\text{BDE}_{\text{standard}}$  is from experimental values or CCSD(T)/CBS computational values, which could be found in Table 2.

The absolute error (AE) reported in this paper is the absolute value of SE; root mean square error (RMSE) refers to

**Table 2.** CCSD(T)/CBS Calculated, Experimental BDEs, and Performance of Several DFT Methods (DFT/mVTZ for Single-Point Calculations and PBE0/VDZ for Geometry Optimization) (Unit: kcal/mol)

no.	complexes	CBS calc.	expt.	B3LYP	PBE0	$\omega$ B97x-D
1	Ag–H	53.2	55.0 <sup>16</sup>	53.6	51.2	54.7
2	Ag–O	45.5	46.4 <sup>17</sup>	45.7	44.4	46.8
3	Ag–F	81.7	82.3 <sup>16</sup>	76.1	75.3	80.0
4	Ag–S	52.5	51.8 <sup>16</sup>	49.7	52.3	54.3
5	Ag–Cl	75.7	75.1 <sup>16</sup>	68.0	71.9	74.7
6	Ag–CH <sub>3</sub>	42.8 <sup>a</sup>	32.1 <sup>16</sup>	39.4	40.9	43.4
7	Ag–OH	56.3 <sup>a</sup>		50.3	50.6	54.3
8	Ag–Br	69.9	70.0 <sup>16</sup>	62.1	66.0	67.0
9	Ag–I	63.9 <sup>a</sup>	60.9 <sup>16</sup>	56.1	60.2	60.9
10	Ag–Se	50.0	50.2 <sup>16</sup>	47.1	49.2	51.2
11	Ag–Te	48.4	46.8 <sup>16</sup>	44.7	46.9	49.4
12	Ag–Si	42.5	44.2 <sup>16</sup>	42.6	42.6	42.9
13	Ag–Ge	40.2	41.7 <sup>16</sup>	40.7	39.9	42.6
14	Ag–Sn	40.3 <sup>a</sup>	32.5 <sup>16</sup>	39.7	39.0	42.6
	RMSE			4.5	3.3	1.9

<sup>a</sup>As benchmark value.

the root mean square of SE; and mean SE (MSE) and mean AE (MAE) discussed below are the means of the SE and AE, respectively.

According to Luo's CRC Comprehensive Handbook of Chemical Bond Energies<sup>16</sup> and related literature,<sup>17</sup> 14 experimental Ag–X bond energies were collected to examine the performance of different theoretical methods (Tables 2 and S6). First, CCSD(T) with complete basis set (CBS) (derived from a  $3\xi/4\xi$  two-point extrapolation, more calculation details shown in the Supporting Information) was found to accurately predict the Ag–X bond energies with an error of <2.0 kcal/mol ( $R^2 = 0.99$ ,  $N = 10$  while the fixed slope is 1, Figure S3) with the exception of BDE(Ag–CH<sub>3</sub>), BDE(Ag–OH), BDE(Ag–Sn), and BDE(Ag–I). The calculated BDE(Ag–CH<sub>3</sub>)<sub>CBS</sub> is 42.8 kcal/mol, which deviates much from the experimental values as observed previously by Chen<sup>18</sup> and Rijs<sup>10</sup> et al. Considering the good agreement between the theoretical and the experimental results for the other silver systems, the experimental BDE(Ag–CH<sub>3</sub>) might need further validation. Herein, for Ag–CH<sub>3</sub>, Ag–OH and Ag–I, and Ag–Sn, the BDEs calculated using CCSD(T)/CBS were judged as the most appropriate benchmark. In contrast, BP86 and PBE0 previously used by Hii and Chattaraj performed with the RMSEs of 4.5 and 3.3 kcal/mol, respectively. For MP2 and DFT methods, the mVTZ (may-cc-pVTZ for H, C, O, S, F, Si, and Cl; may-cc-pVTZ-PP for Ge, Sn, Se, Te, Br, and I; and cc-pVTZ-PP for Ag) basis sets were used.<sup>19</sup>

Based on Figure 1, we conclude that the theoretical protocol PBE0/VDZ// $\omega$ B97x-D/mVTZ could accurately predict the homolytic BDEs of Ag–X complexes with a precision of 1.9 kcal/mol. A more detailed diagram (Figure S4) and related analysis of different functionals could be seen in the Supporting Information.

### 2.3. Calculations of Different Ag–C and Ag–O BDEs.

With the screened theoretical protocol in hand, a series of Ag complexes mainly including Ag–C and Ag–O bonds were selected for further investigation, which might be the key intermediates involved in the transition-metal catalyzed C–H activation and decarboxylation. The calculated BDE(Ag–C)

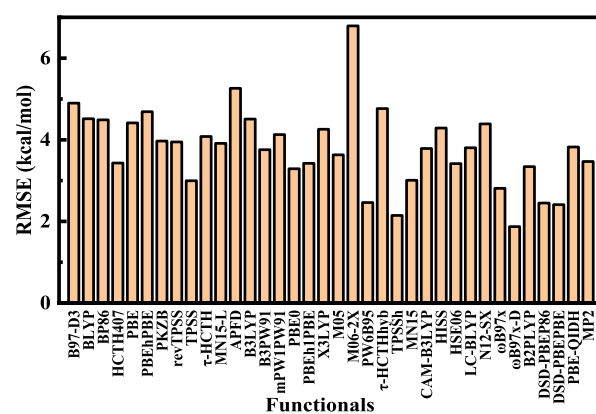


**Figure 1.** Performances of different methods involving DFT functionals and MP2 (DFT/mVTZ for single-point calculations and PBE0/VDZ for geometry optimization).

and BDE(Ag–O) results are summarized in Tables 3 and 4, respectively.

As shown in Figure 2, the BDE (Ag–X) ( $X = C$  and  $O$ ) covers a wide range from 15 to 70 kcal/mol. In detail, BDE(Ag–C<sub>alkyl</sub>) is generally from 27 to 47 kcal/mol, while BDE(Ag–C<sub>aryl</sub>) ranges from 45 to 69 kcal/mol. The BDE(Ag–C<sub>alkyl</sub>) turned out to be generally higher compared to BDE(Ag–C<sub>aryl</sub>). It is thus suggested that the cleavage of the Ag–C<sub>alkyl</sub> bond could easily go through a radical process rather than Ag–C<sub>aryl</sub>. For Ag–O, BDE(Ag–OCOPhX) bond energies occupied a narrow scale from 64 to 70 kcal/mol, much smaller than BDE(Ag–OPhX), which ranges from 19 to 39 kcal/mol. It is worth noting that with the same substituents, BDE(Ag–PhX), BDE(Ag–OPhX), and BDE(Ag–OCOPhX) range from 51 to 54, 19 to 39, and 64 to 70 kcal/mol, respectively. It indicated that the intermediates Ag–OCOPhX may undergo decarboxylation generating an Ag–PhX complex instead of generating Ag–OPhX.

**2.4. Hammett-Type Analysis of Reactivity Parameters.** Based on a linear free-energy relationship theory, the Hammett constant was quantitatively applied to describe the substituent effect on reactivity.<sup>21–23</sup> In addition to the para Hammett constants  $\sigma$ , natural population analysis (NPA) charge on the Ag atom was chosen to explore the quantitative correlation with the reactivity parameters, such as BDE(Ag–O) and decarboxylation barriers.

**2.5. Correlation of Hammett Constants with BDE(Ag–O).** In terms of Ag–OPhX ( $X = \text{NH}_2$ , OMe, Me, H, Cl, and NO<sub>2</sub>) complexes, a linear relation was found between the Hammett constants and the BDE(Ag–OPhX), as shown in Figure 3. The correlation coefficient  $R^2$  is 0.9449. This means that the electron-donating substituents on the benzene ring could promote the homolytic cleavage of the Ag–OPhX bond to afford a radical process. Correspondingly, the NPA charges on Ag of Ag–OPhX (listed in Table 4) were found to correlate well with the BDE(Ag–OPhX) with a correlation coefficient  $R^2$  of 0.9678, as shown in Figure 4 and eq 6. Most likely, the electron-donating substituents in Ag–OPhX weaken the polarization of the Ag–O bond.

$$\text{BDE(Ag–OPhX)} = 28.57 + 13.32\sigma \quad R^2 = 0.9449 \quad (5)$$

Table 3. Calculated Bond Energies of Different Ag–C Complexes (Unit: kcal/mol)

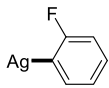
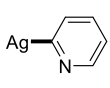
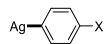
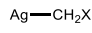
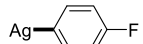
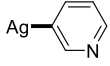
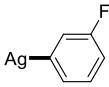
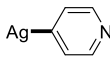
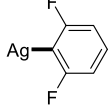
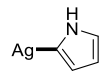
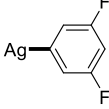
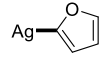
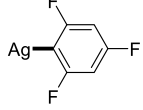
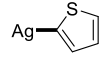
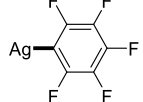
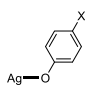
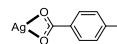
Structures	BDE	Structures	BDE	Structures	BDE	Structures	BDE
	57.5		46.0				
				R=-NH <sub>2</sub>	51.7	R=-NH <sub>2</sub>	30.6
	52.5		53.5	-OMe	51.9	-OMe	32.4
	52.1		52.0	-Me	51.2	-Me	37.5
	64.5		61.2	-H	51.0	-H	43.2
	53.2		62.3	-Cl	52.6	-Cl	38.2
	65.9		61.7	-NO <sub>2</sub>	53.7	-NO <sub>2</sub>	46.6
	68.4						

Table 4. Hammett Constant, NPA Charge on Ag, and Calculated Bond Energies of Different Ag–O Complexes

Substituent	Hammett constant $\sigma_{\text{para}}^{20}$	BDE(Ag–O) (kcal/mol)			
		NPA charge on Ag		NPA charge on Ag	
-NH <sub>2</sub>	-0.66	0.745	19.4	0.801	64.9
-OMe	-0.27	0.761	22.9	0.804	65.8
-Me	-0.17	0.782	28.0	0.805	66.2
-H	0	0.784	30.6	0.807	66.7
-Cl	0.23	0.793	30.7	0.812	67.9
-NO <sub>2</sub>	0.78	0.809	38.6	0.820	70.0

$$\text{BDE}(\text{Ag}-\text{OPhX}) = -198.02 + 290.62 \cdot \text{NPA} \quad (6)$$

$$R^2 = 0.9678$$

Furthermore, again, a good linear correlation was addressed between the BDE(Ag–OCOPhX) and the Hammett constants (Figure 5) as well as the NPA charges on Ag (Figure 6). The correlation coefficients  $R^2$  amount to 0.9808 and 0.9979,

respectively. According to eqs 5 and 7, the slopes are 13.32 and 3.65 for Ag–OPhX and Ag–OCOPhX complexes, respectively. It turned out that the electronic properties of the substituents could affect the BDE(Ag–O) more for Ag–OPhX rather than for Ag–OCOPhX. This may be attributed to the different hapticities on the Ag center. For Ag–OPhX and Ag–OCOPhX, the hapticities are  $\eta^1$  and  $\eta^3$ , respectively. With

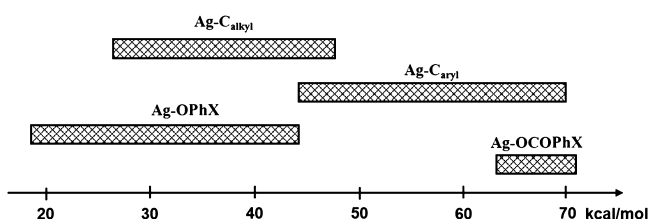


Figure 2. Ranges of BDE(Ag-C) and BDE(Ag-O).

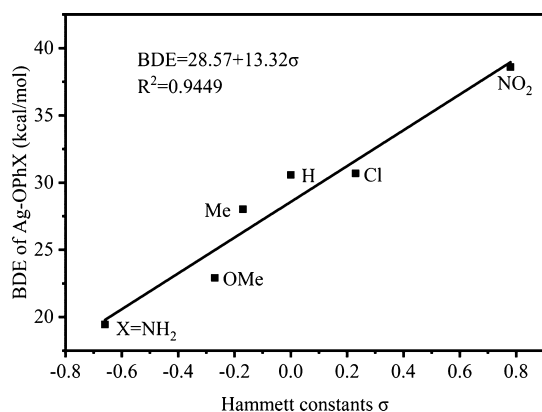


Figure 3. BDE(Ag-OPhX) with different substituents plotted against the Hammett constants  $\sigma$

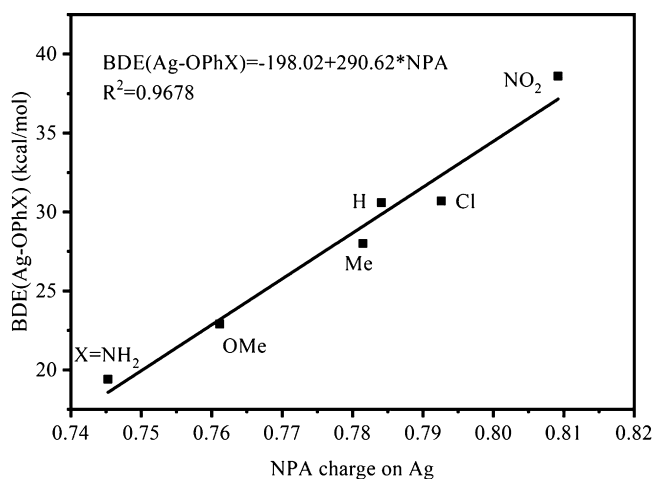


Figure 4. BDE(Ag-OPhX) with different substituents plotted against the NPA charges on Ag.

three atoms O, C, and O bound to the Ag atom, the electronic effect of the substituents could be attenuated. Moreover, compared with Ag-OPhX, the NPA charges on the Ag atoms of Ag-OCOPhX are more positively charged (listed in Table 4). Stronger polarization of the Ag-O bond thus prevails, resulting in larger bond energies.

$$\text{BDE}(\text{Ag}-\text{OCOPhX}) = 66.97 + 3.65\sigma \quad R^2 = 0.9808 \quad (7)$$

$$\text{BDE}(\text{Ag}-\text{OCOPhX}) = -151.44 + 270.23*\text{NPA} \quad R^2 = 0.9979 \quad (8)$$

To gain more insights about Ag-O complexes, the BDE(H-O) values for H-OPhX and H-OCOPhX complexes were estimated for comparison. The calculated results are shown in Table S11 and Figures S6 and S7. As we

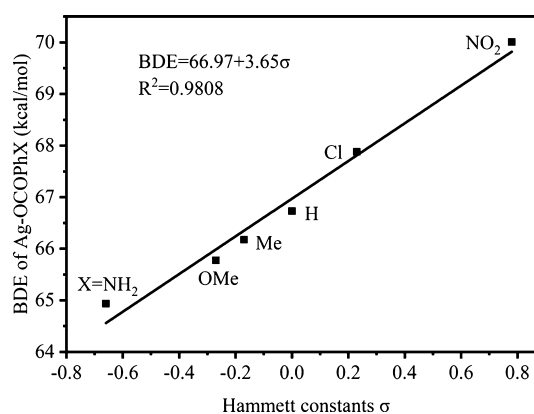


Figure 5. BDE(Ag-OCOPhX) with different substituents plotted against the Hammett constants  $\sigma$

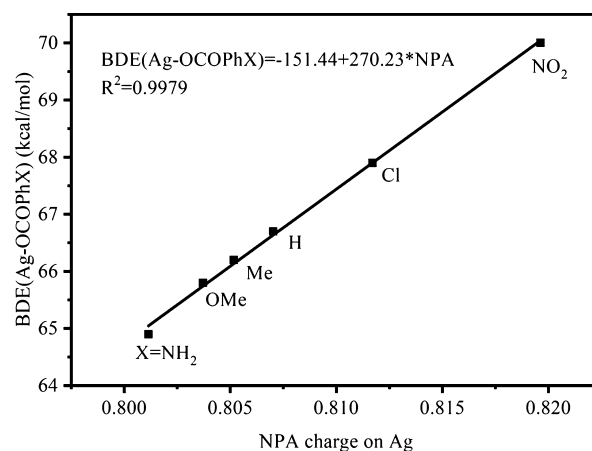


Figure 6. BDE(Ag-OCOPhX) with different substituents plotted against the NPA charges on Ag.

expected, positive linear relationships could be found for BDE(H-O) as well as BDE(Ag-O). According to the fitting results, the slopes of Hammett plots are 8.50 and 1.49 for HOPhX and HOCOPhX systems, respectively. In comparison, the slopes of Hammett plots are 13.32 and 3.65 for Ag-OPhX and Ag-OCOPhX systems, much larger than those for HOPhX and HOCOPhX. It was indicated that except for the stability trends of radicals, the polarizability of the substituent on Ag-O bonds might play a more important role in the homolytic cleavage.

$$\text{BDE}(\text{H}-\text{OPhX}) = 83.56 + 8.50\sigma \quad R^2 = 0.9069 \quad (9)$$

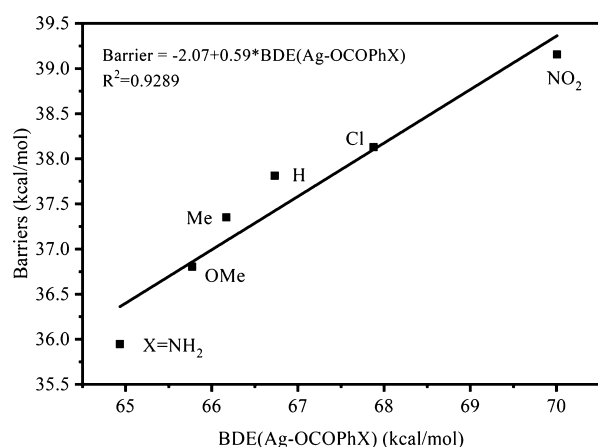
$$\text{BDE}(\text{H}-\text{OCOPhX}) = 107.45 + 1.49\sigma \quad R^2 = 0.9810 \quad (10)$$

**2.6. Correlation of Hammett Constants with Decarboxylation Barriers.** With regard to Pd-catalyzed decarboxylation, both experimental and theoretical works have been extensively reported.<sup>24-27</sup> Not only the R-H gas-phase acidity<sup>24</sup> but also the BDE of R-COOH<sup>25</sup> were found to correlate well with Pd-catalyzed R-COOH decarboxylation energy barrier. By contrast, little efforts involving Ag-assisted decarboxylation have been made. Herein, with the method PBE0/VDZ// $\omega$ B97x-D/mVTZ, silver-assisted decarboxylation barriers  $\Delta H^\ddagger$  were calculated, as listed in Table 5. The structures of the key intermediates and related transition states are presented in Table S11. A linear relationship was found

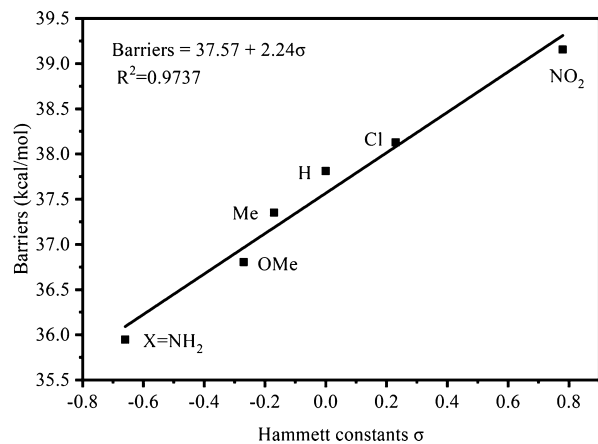
**Table 5. Theoretical Activation Enthalpies of Ag-Assisted Decarboxylation with Different Substituents**

substituent X	Hammett constant $\sigma_{\text{para}}$ <sup>20</sup>	$\Delta H_{\text{decarboxylation}}^{\ddagger}$ (kcal/mol)
-NH <sub>2</sub>	-0.66	35.9
-OMe	-0.27	36.8
-Me	-0.17	37.4
-H	0	37.8
-Cl	0.23	38.1
-NO <sub>2</sub>	0.78	39.2

between the decarboxylation barriers and the BDE(Ag-OCOPhX) with a correlation coefficient  $R^2$  of 0.9289, as shown in Figure 7. It revealed that the Ag-OCOPhX complex

**Figure 7.** Decarboxylation barriers with different substituents plotted against BDE(Ag-OCOPhX).

with small BDE(Ag-O) was inclined to undergo a decarboxylation process. Interestingly, a better linear relationship was also found between the Hammett constants and the reactivity with a correlation coefficient  $R^2$  of 0.9737, as shown in Figure 8. The intercept of eq 12 represents the decarboxylation barrier of Ag-OCOPh with a value of 37.57 kcal/mol. Last but not the least, it suggests that electron-donating substituents could be of benefit for Ag-assisted decarboxylation.

**Figure 8.** Decarboxylation barriers with different substituents plotted against Hammett constants  $\sigma$ .

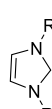
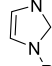
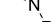
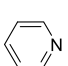
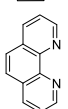
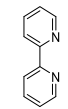
$$\text{barriers} = -2.07 + 0.59 * \text{BDE}(\text{Ag}-\text{OCOPhX})$$

$$R^2 = 0.9289 \quad (11)$$

$$\text{barriers} = 37.57 + 2.24\sigma \quad R^2 = 0.9737 \quad (12)$$

**2.7. Ligand Effects on BDE(LAg-H).** Transition-metal hydrides do not only serve as a hydride donor but also play a crucial role in the hydrogen atom transfer process.<sup>28–30</sup> Uddin et al.<sup>31</sup> systematically investigated the intrinsic nature of the  $L_nM-H$  ( $M = \text{group } 10-11 \text{ metals}$ ) bond and the relationship with dissociation enthalpies. Herein, BDE(Ag-H) and NPA charges on Ag were calculated with various ligands, such as P-ligands, carbene ligands, and N-ligands so forth (Table 6).

**Table 6. Calculated Ag-H Bond Energies with Different Ligands**

Ligands	NPA charges on Ag	BDE(LAg-H) (kcal/mol)
—	0.358	54.7
CO <sub>2</sub>	0.334	59.6
H <sub>2</sub> O	0.301	66.7
CO	0.253	71.4
R=H	0.224	73.1
PR <sub>3</sub> R=Me	0.184	75.8
R=Ph	0.219	75.1
 R=H	0.202	79.0
 R=Me	0.198	79.4
 R= CMe <sub>3</sub>	0.184	79.7
NH <sub>3</sub>	0.272	72.3
	0.293	73.2
	0.307	74
	0.309	74.5

Note that the silver hydride without ligands has the lowest homolytic Ag-H BDE. Ligands coordinated to the Ag centers could increase the electron densities located at Ag, leading to strengthening of the Ag-H bond. In particular, in the cases of P-ligands, carbene ligands, and other small molecule ligands (i.e., CO, CO<sub>2</sub>, and H<sub>2</sub>O), it is surprising that a good negative linear relationship was found between the NPA charges on Ag and the BDE(Ag-H) with a correlation coefficient  $R^2$  of 0.9509, as shown in Figure 9. In contrast, N-ligands could have

a positive effect on the BDE(Ag–H). In this case, the correlation coefficient is 0.9555 (Figure 9).

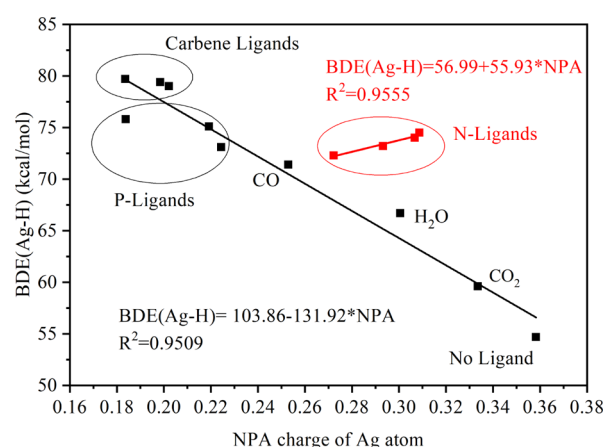


**Figure 9.** BDE(Ag–H) with different ligands plotted against NPA charges on Ag atoms.

### 3. CONCLUSIONS

The breakage and generation of Ag–X (X = C, O, and H) bonds are the vital processes in silver-catalyzed/-assisted C–H activation/decarboxylation. However, the basic knowledge of the structure–reactivity relationship between Ag–X bond energy and reactivity parameters was still unclear. To achieve this goal, we found that the theoretical protocol PBE0/VDZ// $\omega$ B97x-D/mVTZ could accurately predict the homolytic BDEs of Ag–X complexes with a precision of 1.9 kcal/mol by benchmarking 37 calculation methods against the available experimental bond length and energy data. With the aid of such a procedure, a wide range of different Ag–X BDEs were estimated. It is worth noting that with the same substituents, BDE(Ag–CH<sub>2</sub>X), BDE(Ag–PhX), BDE(Ag–OPhX), and BDE(Ag–OCOPhX) (X = NH<sub>2</sub>, OMe, Me, H, Cl, and NO<sub>2</sub>) were in the ranges of 27–47, 51–54, 19–39, and 64–70 kcal/mol, respectively. Subsequently, Hammett-type analysis was conducted for reactivity parameters. Good positive linear relationship was found for BDE of Ag–O bands and decarboxylation barriers of Ag–OCOPhX with the Hammett constants  $\sigma$ . It suggested that electron-donating substituents could promote either the homolytic cleavage of the Ag–OPhX bond to undergo a radical process or Ag–OCOPhX decarboxylation. Moreover, ligand effects on Ag–H bonds were investigated with NPA charges on Ag and BDE(Ag–H). In the case of P-ligands, carbene ligands, and other small molecule ligands (i.e., CO, CO<sub>2</sub>, and H<sub>2</sub>O), a good negative linear relationship was found. In contrast, N-ligands could have a reverse effect.

### 4. METHODS

**4.1. Computational Details.** All the computational studies were performed with Gaussian 16, Revision C.01.<sup>32</sup> All the geometries were optimized in the gas phase without any constraints and confirmed as true energy minima by analysis of the vibrational frequencies at the same level of theory. For molecules or clusters with multiple relatively stable conformations, different initial conformations were given to find the most stable conformation with the lowest energy. For the single-point energy calculations of DFT (excluding the double

hybrid functional) and HF methods, the keyword “stable” was used to ensure the stability of wave functions. The NPA was performed to obtain NPA charge using the NBO 3.1 program<sup>33</sup> as implemented in the Gaussian 16, Revision C.01.

### ■ ASSOCIATED CONTENT

#### Supporting Information

The Supporting Information is available free of charge at <https://pubs.acs.org/doi/10.1021/acsomega.1c05563>.

More computational details; related benchmark results of Ag–X bond lengths; BDE calculations of CCSD(T)/CBS; geometries of optimized silver-containing compounds, intermediates, and transition states; and calculated BDE(H–OPhX) and BDE(H–OCOPhX) (PDF)

### ■ AUTHOR INFORMATION

#### Corresponding Authors

**Shi-Ya Tang** – SINOPEC Research Institute of Safety Engineering, Qingdao 266000, P. R. China; State Key Laboratory of Safety and Control for Chemicals, Qingdao 266000, P. R. China; Email: [tangsy.qday@sinopec.com](mailto:tangsy.qday@sinopec.com)

**Shaodong Zhou** – Zhejiang Provincial Key Laboratory of Advanced Chemical Engineering Manufacture Technology, College of Chemical and Biological Engineering, Zhejiang University, Hangzhou 310027, P. R. China; [orcid.org/0000-0003-3048-4678](https://orcid.org/0000-0003-3048-4678); Email: [szhou@zju.edu.cn](mailto:szhou@zju.edu.cn)

#### Author

**Lei Wu** – Zhejiang Provincial Key Laboratory of Advanced Chemical Engineering Manufacture Technology, College of Chemical and Biological Engineering, Zhejiang University, Hangzhou 310027, P. R. China; SINOPEC Research Institute of Safety Engineering, Qingdao 266000, P. R. China; State Key Laboratory of Safety and Control for Chemicals, Qingdao 266000, P. R. China

Complete contact information is available at: <https://pubs.acs.org/doi/10.1021/acsomega.1c05563>

#### Notes

The authors declare no competing financial interest.

### ■ ACKNOWLEDGMENTS

The authors acknowledge generous financial support from the National Natural Science Foundation of China (no. 21878265) and Science & Technology R&D Dept. of SINOPEC (no. KL18021).

### ■ REFERENCES

- (1) Panigrahi, A.; Whitaker, D.; Vitorica-Yrezabal, I. J.; Larrosa, I. Ag/Pd Cocatalyzed Direct Arylation of Fluoroarene Derivatives with Aryl Bromides. *ACS Catal.* **2020**, *10*, 2100–2107.
- (2) Shimoyama, Y.; Kuwabara, J.; Kanbara, T. Mechanistic Study of Pd/Ag Dual-Catalyzed Cross-Dehydrogenative Coupling of Perfluoroarenes with Thiophenes. *ACS Catal.* **2020**, *10*, 3390–3397.
- (3) Colletto, C.; Panigrahi, A.; Fernández-Casado, J.; Larrosa, I. Ag(I)-C-H Activation Enables Near-Room-Temperature Direct alpha-Arylation of Benzo[ b]thiophenes. *J. Am. Chem. Soc.* **2018**, *140*, 9638–9643.
- (4) Honjo, Y.; Shibata, Y.; Tanaka, K. Rhodium-Catalyzed [2+1+2+1] Cycloaddition of Benzoic Acids with Dienes through Decarboxylation and C identical with C Triple Bond Cleavage. *Chem.—Eur. J.* **2019**, *25*, 9427–9432.

- (5) Gooßen, L. J.; Linder, C.; Rodriguez, N.; Lange, P. P.; Fromm, A. Silver-catalysed protodecarboxylation of carboxylic acids. *Chem. Commun.* **2009**, *46*, 7173–7175.
- (6) Gooßen, L. J.; Rodriguez, N.; Linder, C.; Lange, P. P.; Fromm, A. Comparative Study of Copper- and Silver-Catalyzed Protodecarboxylations of Carboxylic Acids. *ChemCatChem* **2010**, *2*, 430–442.
- (7) Zheng, Q.-Z.; Jiao, N. Ag-catalyzed C-H/C-C bond functionalization. *Chem. Soc. Rev.* **2016**, *45*, 4590–4627.
- (8) Minenkova, I.; Sliznev, V. V.; Cavallo, L.; Minenkov, Y. Gas Phase Silver Thermochemistry from First Principles. *Inorg. Chem.* **2019**, *58*, 7873–7885.
- (9) Romanov, V.; Siu, C.-K.; Verkerk, U. H.; Hopkinson, A. C.; Siu, K. W. M. Bond Dissociation Energies of Solvated Silver(I)-Amide Complexes: Competitive Threshold Collision-Induced Dissociations and Calculations. *J. Phys. Chem. A* **2010**, *114*, 6964–6971.
- (10) Rijs, N. J.; Brookes, N. J.; O'Hair, R. A. J.; Yates, B. F. Theoretical approaches to estimating homolytic bond dissociation energies of organocopper and organosilver compounds. *J. Phys. Chem. A* **2012**, *116*, 8910–8917.
- (11) Wong, V. H. L.; Vummaleti, S. V. C.; Cavallo, L.; White, A. J. P.; Nolan, S. P.; Hii, K. K. M. Synthesis, Structure and Catalytic Activity of NHC-Ag(I) Carboxylate Complexes. *Chem.—Eur. J.* **2016**, *22*, 13320–13327.
- (12) Jana, G.; Pan, S.; Chattaraj, P. K. Binding of Small Gas Molecules by Metal-Bipyridyl Monocationic Complexes (Metal = Cu, Ag, Au) and Possible Bond Activations Therein. *J. Phys. Chem. A* **2017**, *121*, 3803–3817.
- (13) Haynes, W. M. *CRC handbook of chemistry and physics*; CRC press, 2014.
- (14) Tran, F.; Stelzl, J.; Blaha, P. Rungs 1 to 4 of DFT Jacob's ladder: Extensive test on the lattice constant, bulk modulus, and cohesive energy of solids. *J. Chem. Phys.* **2016**, *144*, 204120.
- (15) Car, R. Density functional theory: Fixing Jacob's ladder. *Nat. Chem.* **2016**, *8*, 820–821.
- (16) Luo, Y.-R. *Comprehensive handbook of chemical bond energies*; CRC press, 2007.
- (17) Cooper, G. A.; Kartouzian, A.; Gentleman, A. S.; Iskra, A.; van Wijk, R.; Mackenzie, S. R. Dissociation energies of Ag-RG (RG = Ar, Kr, Xe) and AgO molecules from velocity map imaging studies. *J. Chem. Phys.* **2015**, *143*, 124302.
- (18) Chen, Y.-M.; Armentrout, P. B. Guided Ion Beam Studies of the Reactions of Ag<sup>+</sup> with C<sub>2</sub>H<sub>6</sub>, C<sub>3</sub>H<sub>8</sub>, HC(CH<sub>3</sub>)<sub>3</sub>, and c-C<sub>3</sub>H<sub>6</sub>. *J. Phys. Chem.* **1995**, *99*, 11424–11431.
- (19) Papajak, E.; Zheng, J.; Xu, X.; Leverentz, H. R.; Truhlar, D. G. Perspectives on Basis Sets Beautiful: Seasonal Plantings of Diffuse Basis Functions. *J. Chem. Theory Comput.* **2011**, *7*, 3027–3034.
- (20) Hansch, C.; Leo, A.; Taft, R. W. A Survey of Hammett Substituent Constants and Resonance and Field Parameters. *Chem. Rev.* **1991**, *91*, 165–195.
- (21) Ahraminejad, M.; Ghiasi, R.; Mohtat, B.; Ahmadi, R. Computational investigation of the substituent effect in the [2 + 4] Diels–Alder cycloaddition reactions of HSi≡Si(paraC<sub>6</sub>H<sub>4</sub>X) with benzene. *J. Chin. Chem. Soc.* **2021**, *68*, 806–816.
- (22) Varaksin, K. S.; Szatyłowicz, H.; Krygowski, T. M. Towards a physical interpretation of substituent effect: Quantum chemical interpretation of Hammett substituent constants. *J. Mol. Struct.* **2017**, *1137*, 581–588.
- (23) Hammett, L. P. The Effect of Structure upon the Reactions of Organic Compounds. Benzene Derivatives. *J. Am. Chem. Soc.* **1937**, *59*, 96–103.
- (24) Zhang, S.-L.; Fu, Y.; Shang, R.; Guo, Q.-X.; Liu, L. Theoretical analysis of factors controlling Pd-catalyzed decarboxylative coupling of carboxylic acids with olefins. *J. Am. Chem. Soc.* **2010**, *132*, 638–646.
- (25) Shi, J.; Huang, X.-Y.; Wang, J.-P.; Li, R. A Theoretical Study on C-COOH Homolytic Bond Dissociation Enthalpies. *J. Phys. Chem. A* **2010**, *114*, 6263–6272.
- (26) Yan, B.; Zuo, L.; Chang, X.; Liu, T.; Cui, M.; Liu, Y.; Sun, H.; Chen, W.; Guo, W. Kinetically Controllable Pd-Catalyzed Decarboxylation Enabled [5 + 2] and [3 + 2] Cycloaddition toward Carbocycles Featuring Quaternary Carbons. *Org. Lett.* **2021**, *23*, 351–357.
- (27) Yang, X.; Chen, X.; Xu, Y.; Zhang, M.; Deng, G.; Yang, Y.; Liang, Y. Palladium-Catalyzed [4 + 3] or [2 + 2 + 3] Annulation via C-H Activation and Subsequent Decarboxylation: Access to Heptagon-Embedded Polycyclic Aromatic Hydrocarbons. *Org. Lett.* **2021**, *23*, 2610–2615.
- (28) Wang, Y.; Dong, B.; Wang, Z.; Cong, X.; Bi, X. Silver-Catalyzed Reduction of Quinolines in Water. *Org. Lett.* **2019**, *21*, 3631–3634.
- (29) Shevick, S. L.; Wilson, C. V.; Kotesova, S.; Kim, D.; Holland, P. L.; Shenvi, R. A. Catalytic hydrogen atom transfer to alkenes: a roadmap for metal hydrides and radicals. *Chem. Sci.* **2020**, *11*, 12401–12422.
- (30) Wang, L.; Xiao, J. Hydrogen-Atom Transfer Reactions. *Top. Curr. Chem.* **2016**, *374*, 17.
- (31) Uddin, J.; Morales, C. M.; Maynard, J. H.; Landis, C. R. Computational Studies of Metal-Ligand Bond Enthalpies across the Transition Metal Series. *Organometallics* **2006**, *25*, 5566–5581.
- (32) Frisch, M.; Trucks, G.; Schlegel, H.; Scuseria, G.; Robb, M.; Cheeseman, J.; Fox, D. *Gaussian 16*, Revision C. 01; Gaussian, Inc., 2016.
- (33) Glendening, E.; Reed, A.; Carpenter, J.; Weinhold, F., *NBO version 3.1*, TCI; University of Wisconsin: Madison, 1998; Vol. 65.